Burst temperature from conditional analysis in Texas Helimak and TCABR tokamak

F. A. C. Pereira, W. A. Hernandez, D. L. Toufen, Z. O. Guimarães-Filho, I. L. Caldas, and K. W. Gentle

Citation: Physics of Plasmas **25**, 042301 (2018); doi: 10.1063/1.5025062
View online: https://doi.org/10.1063/1.5025062
View Table of Contents: http://aip.scitation.org/toc/php/25/4
Published by the American Institute of Physics

Burst temperature from conditional analysis in Texas Helimak and TCABR tokamak

F. A. C. Pereira,[1] W. A. Hernandez,[1,2] D. L. Toufen,[3] Z. O. Guimarães-Filho,[1] I. L. Caldas,[1] and K. W. Gentle[4]

[1]*Institute of Physics, University of São Paulo, São Paulo, São Paulo 05315-970, Brazil*
[2]*Facultad de Ciencias Básicas e Ingenierías, Universidad de los Llanos, Villavicencio 500017, Colombia*
[3]*Federal Institute of Education, Science and Technology of São Paulo - IFSP, Guarulhos, São Paulo 07115-000, Brazil*
[4]*Department of Physics and Institute for Fusion Studies, The University of Texas at Austin, Austin, Texas 78712, USA*

(Received 6 February 2018; accepted 19 March 2018; published online 2 April 2018)

The procedure to estimate the average local temperature, density, and plasma potential by conditionally selecting points of the Langmuir probe characteristic curve is revised and applied to the study of intermittent bursts in the Texas Helimak and TCABR tokamak. The improvements made allow us to distinguish the burst temperature from the turbulent background and to study burst propagation. Thus, in Texas Helimak, we identify important differences with respect to the burst temperature measured in the top and the bottom regions of the machine. While in the bottom region the burst temperatures are almost equal to the background, the bursts in the top region are hotter than the background with the temperature peak clearly shifted with respect to the density one. On the other hand, in the TCABR tokamak, we found that there is a temperature peak simultaneously with the density one. Moreover, the radial profile of bursts in the top region of Helimak and in the edge and scrape-off layer regions of TCABR shows that in both machines, there are spatial regions where the relative difference between the burst and the background temperatures is significant: up to 25% in Texas Helimak and around 50% in TCABR. However, in Texas Helimak, there are also regions where these temperatures are almost the same. *Published by AIP Publishing.*
https://doi.org/10.1063/1.5025062

I. INTRODUCTION

The turbulence on the plasma border and scrape-off layer (SOL) of magnetically confined devices presents intermittent density peaks, the so-called bursts. These bursts are associated with coherent structures with a plasma density much higher than the average and are responsible for an important part of the particle and energy transport.[1–3] These events affect plasma confinement in nuclear fusion machines, and their characteristics measurement contribute to evaluating the plasma performance.

Basic plasma machines, with highly reproducible discharges and a large number of electrostatic probes,[4–6] also have bursts and present favorable conditions to investigate the burst main characteristics. The Texas Helimak,[7] an example of this kind of machine, has many properties in common with the SOL region of tokamaks: open magnetic lines, magnetic and flow shears, and turbulence with many extreme events. Small tokamaks, such as TCABR,[8] are also interesting machines to investigate bursts as it is possible to use electrostatic probes up to the plasma column border.

Usually, turbulence studies involve several data analysis methods. One of these methods is the statistical analysis of the turbulent signal, applied to estimate statistical characteristics such as turbulence level, skewness, and kurtosis, which are used to infer general fluctuation properties of the turbulent regime.[9–11] Other methods, based on spectral analysis, are applied to identify coherent modes and non-linear coupling between these modes[12] and to estimate the signal stochastic properties.[13]

Another important tool to study the intermittent bursts is the conditional analysis,[14,15] developed to analyze how the system behaves when a certain special event happens. When the chosen event is the extreme density burst, the average burst shape and propagation properties can be determined.[4,5,18,19]

The burst small size and short lifetime pose a hard challenge for the typical diagnostic applications, especially for the temperature and plasma potential determination. The burst plasma potential is used to investigate burst propagation mechanisms and to estimate the burst contribution to the total turbulent transport. The burst temperature is important to evaluate the burst contribution to the energy transport.

Using conditional analysis, the burst temperature and plasma potential can be estimated by detecting bursts in one probe and conditionally fitting probe characteristic curves measured in nearby probes. The conditional fitting involves Langmuir probes configured in ion saturation and voltage sweep modes and can be applied using regular Langmuir probes. This method was applied to turbulence data from TORPEX,[6] for studying the burst generation mechanism, and ASDEX Upgrade,[19] where the influence of the temperature fluctuations on turbulence was investigated.

In this work, we use the large set of probes in Texas Helimak to investigate the burst spatial properties through conditional analysis. For that, we apply the conditional fitting on the probe characteristic curves to characterize the

Texas Helimak bursts. We modify the conditional fitting technique to improve its precision and reliability by combining the conditional selected data with information obtained from the whole time-series probe characteristic curve. We apply this procedure to a grid of probes to estimate the spatial structure of temperature modifications inside the bursts over a radial region of the Texas Helimak and to evaluate how this temperature change can affect the determination of the plasma potential. After that, we analyzed the burst signals in the plasma border and the SOL region of the tokamak TCABR and compared them with the Texas Helimak results.

In Sec. II, we introduce the Texas Helimak and present its main characteristics. In Sec. III, we discuss the characteristic curve conditional fitting and present the improvements we made in this method. In Sec. IV, we apply this method to study the temperature spatio-temporal profile on the Texas Helimak plasma during bursts. In Sec. V, we use the same analysis on the TCABR turbulence data and compare the burst characteristics on both machines. A summary of the results focused on the similarities and differences observed in both machines is presented in Sec. VI.

II. THE TEXAS HELIMAK

The Texas Helimak is a toroidal machine with helical magnetic field lines with curvature and shear [Fig. 1(a)]. The Texas Helimak has a vacuum vessel with a rectangular cross section of internal and external radii 0.6 m and 1.6 m, respectively, and 2 m height, and in the discharges considered here, it was heated by a microwave source with a power of 6 kW at 2.4 GHz, coupled through a window located at the internal radius of the machine. The gas used in these experiments is Argon at 1.3 mPa, and the toroidal field is about 0.1 T with a connection length of several meters (about 40 m at the middle of the machine, $R = 1.1$ m). The magnetic field lines terminate on four sets of plates (located on the top and bottom of the machine). These plates are also used to impose an external electric potential (bias) and are the mechanical support for more than 700 Langmuir probes. The Texas Helimak has a typical shot duration of 20 s. The data analyzed here were taken at the stationary phase of the plasma discharge during

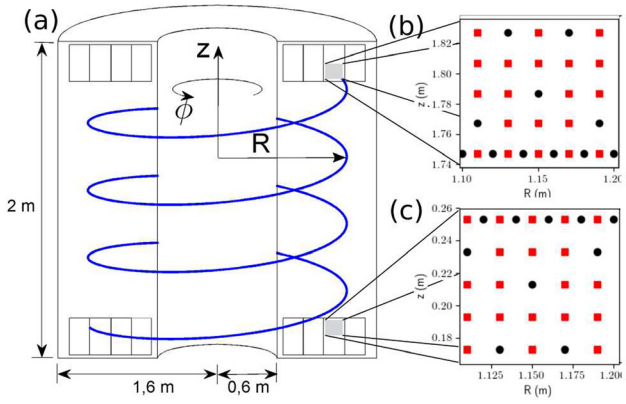

FIG. 1. (a) Texas Helimak vacuum chamber showing a sample of the magnetic field lines and the plates used as a support for the Langmuir probes. (b) and (c) The Langmuir probe distributions used in the discharges considered in this work.

10 s and were registered in 96 channel ADCs with a sampling rate of 500 kS/s.

We analyze turbulence in the region with the most extreme event counts and a radial density gradient on the low field side,[16] located on the plate indicated in Fig. 1. The probes were set to allow a bidimensional view of the burst propagation with most of the probes configured in the voltage sweep mode and just a radial line and some key probes of the grid measuring ion saturation current. Examples of the probe setup for the considered top and bottom regions of the machine can be seen in Figs. 1(b) and 1(c). The probes measuring ion saturation current are presented in black circles, and the probes in the voltage sweep mode are in red squares. This configuration allows us to identify the detection time of the extreme events using the ion saturation current measurements and simultaneously evaluate the 2D spatial profiles of temperature, density, and plasma potential.

In the first step, we determine the average electron temperature by using the whole time series from the probe in the voltage sweep mode. For this, we used the four-parameter probe characteristic curve[17]

$$I(V) = I_s\left(\alpha(V - V_f) - 1 + e^{\frac{e(V-V_f)}{kT_e}}\right), \tag{1}$$

where I_s is the ion saturation current, V_f is the floating potential, T_e is the electron temperature, and α is the linear term of the saturated region, which is related to the probe sheath expansion due to the probe biasing voltage.[17] One important detail in this procedure is the choice of the maximum probe potential V_{max} to be considered in the fit since the fitted temperature has a dependence on it. In tokamaks, it is common to select potentials close to the floating potential, but on machines where the plasma is heated by microwave radiation, as in the Texas Helimak, it is recommended to use maximum potentials between $V_f + 0.5T_e/e$ and $V_f + 2.5T_e/e$ in order to reduce the influence of the suprathermal electrons in the fit.[6] The approach used in the Texas Helimak is to find the maximum potential V_{max} for which the exponential term of the fitted current is around 5 ($V_{max} \approx V_f + 1.5T_e/e$).

III. CONDITIONAL FITTING OF THE PROBE CHARACTERISTIC CURVE

The characterization of plasma (or any other physical system) involves determining typical, or most meaningful, parameters. Because of that, the signals average or median are often used in data analysis. However, when we are interested in specific events that happen in the system during short time intervals, the average picture may be meaningless. The conditional analysis is an approach to characterize the system under selected conditions, as, for example, a special event that occurs several times in the system. With this, instead of relying only on typical values based on the whole time series behavior, we can determine the average system behavior when the selected condition is present. This method is especially useful in systems with strong fluctuations, for which the changes in the behavior cannot be distinguished just by seeing what happens in few occurrences of the event,

but the differences must be determined statistically, which is the case of turbulence parameters.

The Texas Helimak turbulence in the analyzed region (low field side) presents an asymmetrical ion saturation current signal probability density function, with a heavy-tail on the positive side.[5] This asymmetry is due to the presence of intermittent extreme event bursts, with density much higher than the average one (up to 10 standard-deviations). Conditional analysis was used to characterize these extreme events by looking at a grid of neighbor probes during time intervals close to the burst detection in the reference probe at the center of the grid. With this approach, the geometric structure and propagation of the bursts were identified.[5,16]

While the burst ion saturation (and density) signature is well known, its driving mechanism and role in the turbulent particle and energy transport are not completely understood. To achieve this understanding, a good estimate of both temperature and plasma potential fluctuations is necessary.

Our approach is similar to those used in Refs. 18 and 19, where the extreme events were detected on one probe measuring ion saturation current, and other probes measuring voltage sweeps were conditionally selected to create the burst characteristic curve.

Figure 2 shows an example of the conditional selection approach: On a reference probe [2(a)], measuring the ion saturation current, we detect the burst instants (selected using a threshold of 2.5 standard deviations above the average), $T_b = \{t_1, t_2, \ldots\}$. On a neighbor probe, with a voltage sweep configuration [Figs. 2(b) and 2(c)], we select only the data instants for which the bursts were detected on the reference probe, i.e., T_b. This way, we can estimate the plasma parameters when the bursts cross the probe grid.

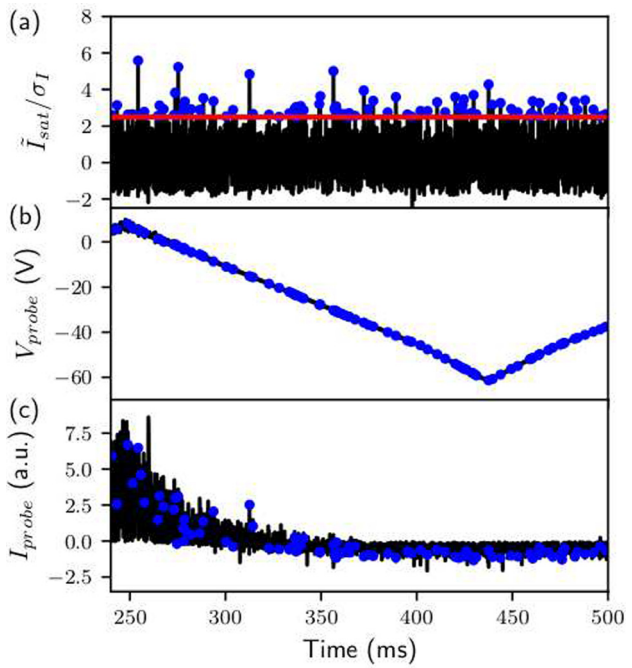

FIG. 2. An example of conditional selection: a reference probe (a) measures ion saturation current, while a second probe has its potential (b) varied in time, and the corresponding probe current is measured (c). The blue dots indicate the instants that bursts are detected at the reference probe.

In Fig. 3, there are two probe characteristic curves, one [Fig. 3(a)] estimated by fitting the whole time series, i.e., the background or typical curve, and the other [Fig. 3(b)] was made using only the burst data [the blue dots in Figs. 2(b) and 2(c)].

The conditional selection involves a huge reduction in the amount of data points (by a factor of 1000) and uses data from the whole acquisition interval, and so, it is important to verify if the curve fitting is both accurate and stable under these conditions. Furthermore, when fitting the characteristic function for the burst data, it may be necessary also to redefine the fitting interval since the floating potential and the temperature may be different during the burst. Therefore, the maximum potential considered in the fit was recalculated using the same criteria used for the whole series (that is $V_{max} \approx V_f + 1.5T_e/e$).

With this approach, we were able to estimate in a consistent way the ion saturation current I_s, the floating potential V_f, and the electron temperature T_e during the presence of the burst. In order to better study the statistical properties of this approach, we did random samplings from the whole series with the same number of data points as the number of bursts, and from each one, we got a set of (I_s, V_f, T_e). By doing that, the fitted parameters are completely unrelated to any special physical process, as the points were randomly chosen, and therefore, the uncertainty of the fitted parameters given by the fit can be compared with their standard deviations among the sets of random samplings.

Figure 4 shows the histograms of V_f, I_s, T_e for 1000 sets of random samplings (each one containing the number of bursts detected in the reference probe). On the left side, we kept the α of Eq. (1) fixed as the value obtained from fitting of the whole series. On the right side, we fitted the four parameters (V_f, I_s, T_e, α) for each dataset. On both methods, the histograms show that the curve-fitted parameters on the

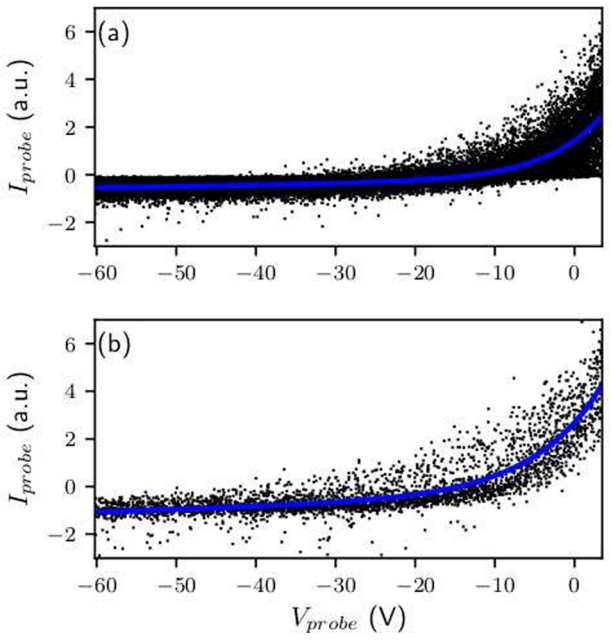

FIG. 3. Example of a probe characteristic curve using all data points (a) and using only the instants that bursts were detected at the reference probe (b).

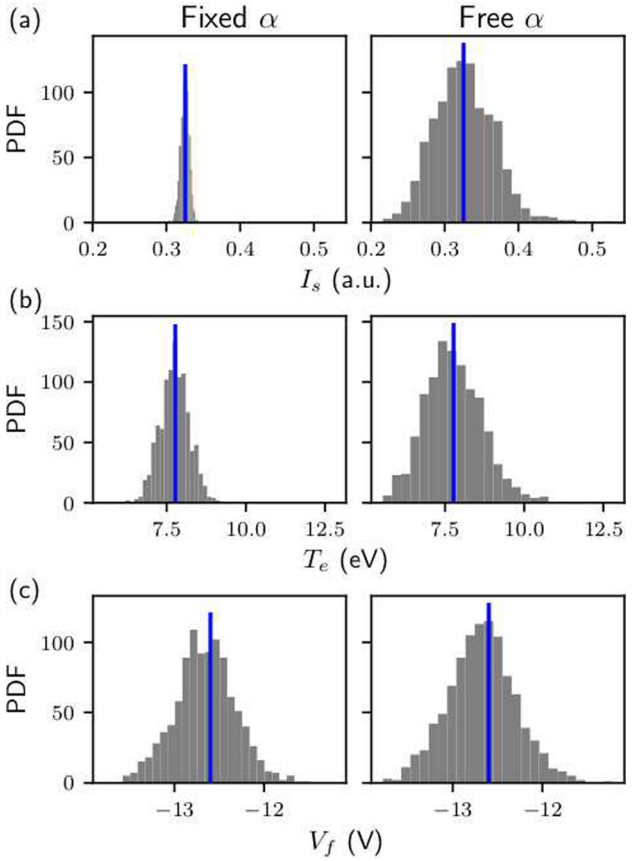

FIG. 4. Histograms of the ion saturation current (a), temperature (b), and floating potential (c) of a thousand random sampled points with the same size of the conditional fitted ones, estimating the parameter α from the curve fitting (right) and using the whole series value (left). The blue vertical lines are the values estimated by fitting all time series points.

reduced datasets fluctuate around the whole series values (the blue lines), and so, the reduction in the amount of data used in the fits does not create any type of statistical biasing or nonsensical result. It only, as expected, increases the uncertainty of the fitted parameters. However, keeping the linear parameter α fixed has a huge effect on the uncertainties of ion saturation and temperature: the ion saturation standard deviation of the four parameters' fitting is seven times higher and the temperature standard deviation is much bigger in the free alpha fittings when compared with the fixed alpha one. Using α as a constant for the conditional fitting also solves a side effect of the reduction in the amount of data used in the fits: due to its large uncertainty, the α parameter obtained from a small amount of data points may result even in negative values.

These histograms also provide another good estimate for the fitted parameter uncertainties: the standard deviation of the histograms. While the parameter uncertainties can be estimated directly from the non-linear least-square fitting, this process can be tricky as the time series fluctuations are correlated in non-trivial ways, and this effect is not considered in the direct estimation of the fitting parameters. For the plasma conditions found in the Texas Helimak, the histogram standard deviations and the parameter uncertainties estimated directly from the fitting are on the same order of magnitude, with the histogram uncertainties being about 50% higher than from the fitting ones for the temperature, 20% higher for the floating potential, and 10% lower for the ion saturation current.

From this analysis, one can see that the conditional fitted values using only data from one shot (about few thousand extreme events with a threshold of 2.5σ) are noisy, as the standard deviation of 0.5 eV makes most of the Texas Helimak burst temperatures somehow compatible with the average. As the Texas Helimak is a machine with reproducible plasma conditions, we solved this problem by taking about ten shots with the same parameters and analyzed them together as if it was a longer shot.

IV. TEMPERATURE CHANGES DUE TO EXTREME EVENTS

In fusion devices, the extreme events at the scrap off layer are expected to be much hotter than the background as they are blobs of matter from the hot plasma interior.[19] However, the Texas Helimak does not have a confined plasma region, and therefore, the temperature differences may not be as high as the ones found in tokamaks.

Figure 5 shows the ion saturation current, the electron temperature, and the plasma and floating potentials estimated by conditional fitting for a target probe 2 cm above the reference probe used to detect the bursts ($t = 0$), located at $r = 1.15$ m and $z = 1.787$ m. The burst conditional fitted temporal profile was obtained by selecting the data points with different delays t with respect to the burst detection time, and then, the characteristic curve was fitted for each delay t. The blue lines are the average values from the ten shots considered. The ion saturation current shows a maximum slightly delayed because the bursts propagate upwards.[16] In the

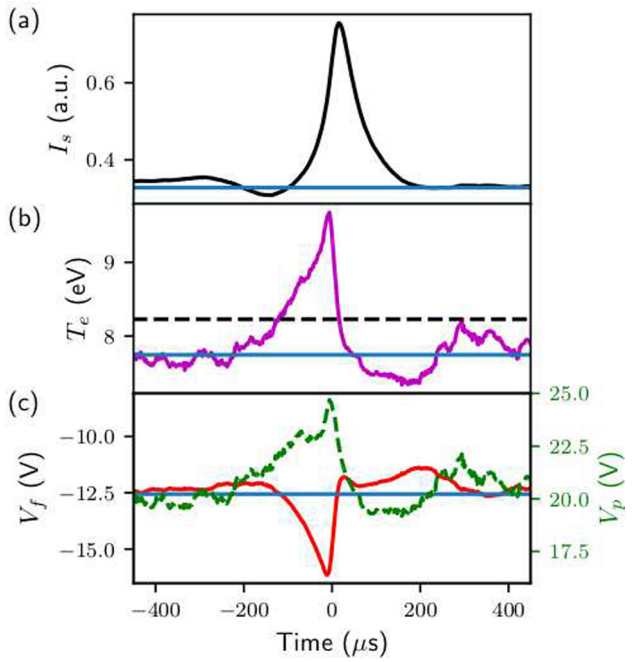

FIG. 5. Conditional fitting: (a) ion saturation current, (b) electron temperature, and (c) floating (red line) and plasma (dashed green line) potential as a function of the delay in relation to the burst instants from the Texas Helimak top region. The horizontal blue lines are the average values for this position.

temperature profile, we can see a 2 eV increase just before the ion saturation current maximum, suggesting that the ion saturation peak is preceded by a temperature rise. The black dashed line corresponds to four standard-deviations of the histogram in Fig. 4(b). To verify the statistical significance of this value, we made temporal profiles for randomly sampled instants and verified the maximum temperature of their time series. The maxima of randomly sampled conditionally fitted time series have a probability of about 2.5% to be above the black dashed line in Fig. 5(b).

One important consequence of this temperature rise is that the floating potential variations have the opposite sign of the plasma potential changes. The calculated plasma potential is shown in Fig. 5(c) (dashed green curve). We estimated the plasma potential using the relation

$$V_p = V_f + \mu \frac{kT_e}{e}, \tag{2}$$

with $\mu = 4.2$, a value determined for a similar machine running with the same gas.[20] The exact value of this parameter does not change the qualitative picture shown in Fig. 5(c): the temperature modification can make the floating potential oscillation completely uncorrelated (or even negatively correlated) with the plasma potential. This effect was also observed using the ASDEX Upgrade.[19]

However, when the same analysis is done for the probes at the machine bottom ($z = 0.213$ m), there is no significant temperature modification, and both floating and plasma potentials increase during the bursts.

As the Texas Helimak has a grid of probes on its plates, we used the conditional fitting analysis on all probes configured in the sweep potential mode. This way, we were able to see the spatial temperature and density fluctuations due to the burst. Figure 6 shows the spatial profile of ion saturation and temperature fluctuations for the probe grid at the bottom and top of the machine when the burst is detected at the reference probe (black dot).

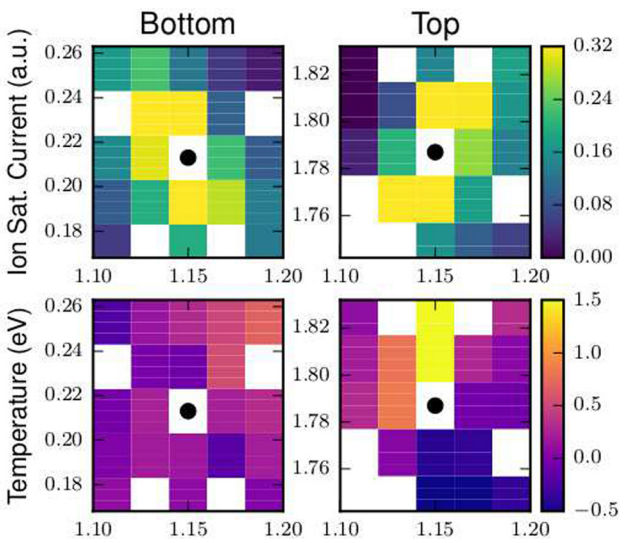

FIG. 6. Fluctuations of ion saturation current and electron temperature conditionally estimated for a grid of probes close to the reference probe (black dots) on top and bottom of the machine.

The ion saturation current shapes (Fig. 6) are the same as if the probes were directly measuring them: an elongated elliptic-like structure that is tilted about 50° with respect to the radial direction with opposite directions in the top and bottom regions of the machine. The inclination difference between top and bottom parts is consistent with the magnetic field line shear at this radial position, corresponding to the horizontal burst at the middle of the machine. The burst shape at the Texas Helimak top is an example of how assuming the propagation direction from delays can lead to erroneous conclusions about the burst velocity: the burst predominant upward movement makes the higher radius probes at the same height of the reference to detect the burst peak before the reference probe, suggesting an inward burst propagation. However, by following the structure propagation with the whole grid, we can see that the burst actually moves outwards.[5]

The temperature profiles, on the other hand, show different behaviors on each end of the machine: at the top, a clear higher temperature region is just ahead of the ion saturation (and density) maximum, while at the bottom of the machine, the temperature change is much smaller, and it is not possible to clearly identify a hotter region. This asymmetry may be due to the plasma flow be upwards in this region, and so, the bottom bursts come from a slightly cooler region close to the machine base wall, while the top bursts come from the machine center.

We analyzed the electron temperature and ion saturation current variation due to bursts for the radial interval considered in this work. The burst maximum temperature and current in the top region of the Texas Helimak are shown in Fig. 7, together with the average values. In Fig. 7(a), we can see that the bursts and average ion saturation current decrease radially, following similar trends. From Fig. 7(b), we can see that the burst temperature profile has two different regions: up to the radius of $R = 1.17$ m, the bursts are considerably hotter than the average. For probes with a radius greater than R = 1.19 m,

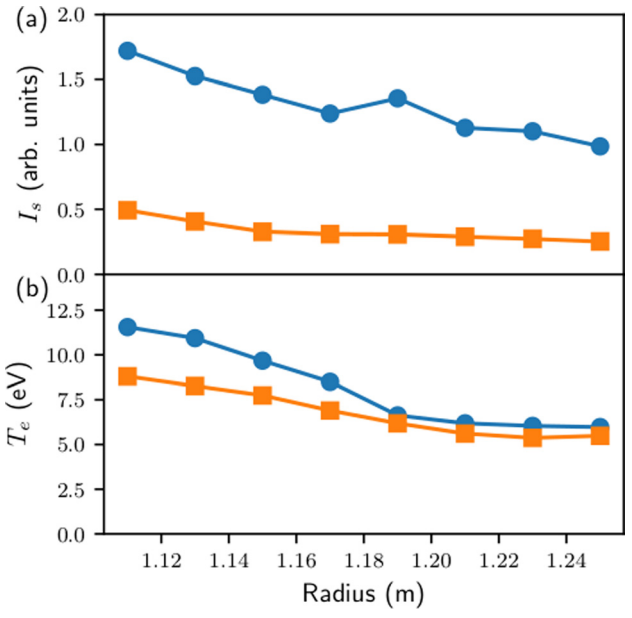

FIG. 7. Radial dependence of the burst (circles) and mean (squares) electron density (a) and temperature (b) for the top region of the Texas Helimak.

it is not possible to clearly identify a hotter region. For the bottom of the machine, the burst temperature is almost equal to the average in the whole analyzed radial interval.

V. BURST TEMPERATURE IN THE TCABR

The TCABR is a tokamak with major radius $R_0 = 0.615$ m, minor radius $a = 0.18$ m, central electron temperature up to 500 eV, a plasma current of 90 kA, and a toroidal magnetic field of 1.07 T. The plasma column has a circular shape delimited by a set of four graphite limiters. Figure 8 shows the schematic representations of the poloidal cross-section of the vessel and plasma column and the frontal view of the 5-pin probe with the configuration used on the analyzed shots. The TCABR shot duration is around 100 ms, with 50 ms of the stationary phase. The turbulence measurements were registered using an ADC system with a sampling rate of 2 MS/s.

The turbulence signal in the TCABR border and scrape-off layer (SOL) also presents an asymmetrical heavy-tailed probability density distribution, with many extreme events where the plasma density can achieve many times its average value.[8] We conditionally selected points on the voltage sweeping probe [V_r on Fig. 8(b)] with the bursts detected on the ion saturation current probe (I_s) and applied the same methodology done on the Texas Helimak (with the exception that $V_{max} = 7.5$ V for the TCABR). With this approach, we obtained the temporal profiles for the burst plasma parameters (ion saturation current, I_s, electron temperature, T_e, and floating potential, V_f).

Figure 9 shows the burst temporal profiles when the 5-pin probe is located at $r = 18.5$ cm or 0.5 cm out of the plasma border. The burst ion saturation current temporal profile matches the typical signature for SOL bursts:[1] fast density rising with a slower decaying time and a duration of about 10 μs. Here, we can see two important differences with respect to the Texas Helimak bursts: the Texas Helimak bursts have a more symmetrical temporal profile, with similar rising and decaying times (the burst decaying times on the TCABR increase as we move further from the plasma border), and the Helimak bursts are much longer, about 200 μs (see Fig. 5). As the perceived duration is strongly linked both with the burst size and velocity, the TCABR (and other

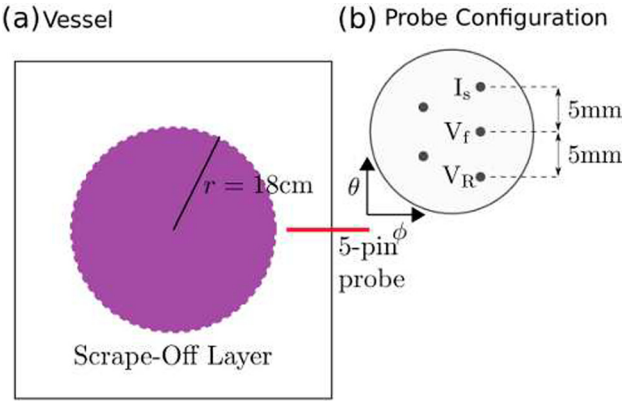

FIG. 8. (a) TCABR vacuum chamber cross section, with the plasma column and the 5-pin probe position. (b) The Langmuir probe distribution used for the discharges considered in this work.

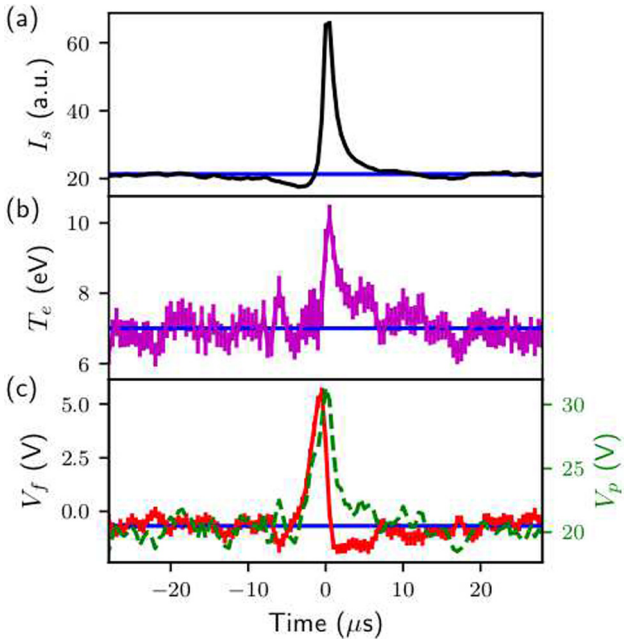

FIG. 9. Conditional fitting: (a) ion saturation current, (b) electron temperature, and (c) floating (red line) and plasma (dashed green line) potential as a function of the delay in relation to the bursts for the TCABR, at an equatorial position of 0.5 cm from the plasma border ($r = 18.5$ cm). The horizontal blue lines are the average values for this position.

tokamaks) bursts are much faster and/or smaller than the Texas Helimak ones.

The TCABR burst temperature profile [Fig. 9(b)] shows a temperature rising (and decaying) synchronized with the ion saturation burst, agreeing with the results from the ASDEX Upgrade.[19] The temperature variation is also higher than the one we found at the Texas Helimak, and the different temporal profile between the two machines indicates that these two structures may have different internal dynamics and origin.

On the other hand, the floating potential of the TCABR bursts [Fig. 9(c)] does not present a negative peak together with the temperature peak, showing only a positive potential maximum just before the burst. Still, assuming that the floating potential fluctuation reflects the plasma potential is misleading, as the floating potential has a peak just before the burst, while the plasma potential follows the burst profile.

We applied this analysis for shots with the probe at different radial positions. In Fig. 10, we show the electron density and temperature for the TCABR border and scrape-off layer. The orange squares are the average values, and the blue circles are the burst values. In both cases, the density and temperature decrease when we move away from the plasma column. For the whole interval, the burst density is about three times the average density at the same position, even inside the column close to the border. The burst temperature is not much bigger than average at the border, but the difference starts being more significant at the SOL.

According to the most accepted models for the burst formation,[3,21–23] the bursts detected at any point in the SOL certainly traveled all the way to that radius as there is no significant burst formation there. So, we can use Fig. 10 to study the diffusion of burst temperature and density and to

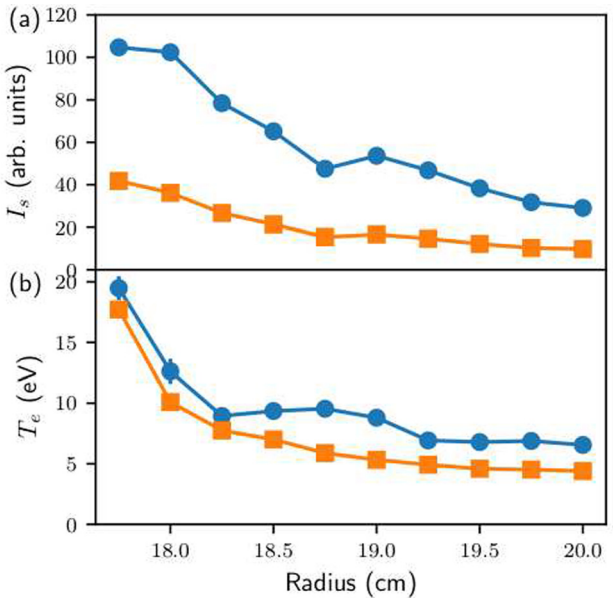

FIG. 10. Radial dependence of the burst (circles) and mean (squares) ion saturation current (a) and electron temperature (b) for the TCABR.

see how it is related to the average scenario at these positions. The density from Fig. 10(a) shows that both bursts and the average decrease by the same pattern, with bursts being about three times denser than the average. This indicates that the burst density has an important contribution to the average density at the SOL.

The electron temperature radial profile [Fig. 10(b)] indicates a slightly different scenario: the electron temperature decreases as we move away from the plasma column, but the burst temperature follows this decrease only up to $r = 18.25$ cm and then decreases much more slowly than the average temperature. It makes bursts at the border just a little bit hotter (about 10%) than the average and much hotter at the SOL (about 50%). So, the bursts maintain their temperature much longer than the average plasma.

VI. CONCLUSIONS

We applied a procedure, based on the conditional analysis of electrostatic probe data, to estimate the burst temperature on Texas Helimak and TCABR tokamak. The procedure combines data from different probes to obtain an average characteristic curve composed of values selected near extreme density events on plasma edge turbulence, and from this curve, we determine the temperature of the density bursts. We improve the precision of this procedure by using the non-conditional value for the term related to the probe sheath region expansion due to biasing in the characteristic curve fitting. This statistical procedure allows us to obtain the electronic temperature with lower uncertainties, which was confirmed by histograms of fitted average temperature from several random sampled data.

Then, we applied this procedure to the Texas Helimak turbulence data from a grid of probes and determined the ion saturation current, floating potential, and electron temperature inside the bursts. As expected, the ion saturation signals are similar to those obtained directly from ion saturation current measurements, showing a 2D structure tilted in opposite directions in the top and the bottom of the machine. Differences between top and bottom were also found in the shape of the burst temperature: the bottom region presents no significant temperature increase during the bursts, while the top has a large increase (20%) shifted with respect to the burst density peak. From the floating potential data, we confirmed that the temperature modifications may even make the floating potential change to be in the opposite direction of the plasma potential one.

We also analyze the bursts in the TCABR plasma border and scrape-off layer regions. When applying this procedure to the TCABR data, we observed a temperature peak synchronized with the density burst, as seen at ASDEX Upgrade,[19] where the density bursts come from a denser and hotter plasma interior. While in the TCABR the floating and plasma potential variations during the bursts do not have different signs, the temperature effects are large enough to compromise the use of the floating potential instead of the plasma potential for electric field determinations, especially inside the bursts.

While the bursts in both machines have similar density properties (temporal profiles and statistics), the burst temperature properties are different: the TCABR bursts fit the typical image: denser and hotter blobs of plasma detached from the plasma column traveling ballistically towards the wall. On the other hand, in Texas Helimak, where all magnetic field lines are connected with the wall, the bursts do not fit well this description: the burst temperature maximum does not coincide with the density maximum or it has the same temperature of the background.

The TCABR and Texas Helimak burst ion saturation current radial profiles have a similar radial dependence as the average ion saturation current, as one can expect because of the way they are detected. However, the temperature profiles show a different behavior: in the Texas Helimak top region, the bursts go from significantly hotter at $R = 1.11$ m to the same temperature from $R = 1.19$ m on, while at TCABR, the temperature difference increases at the start of the SOL and keeps being significant in the whole analyzed interval.

ACKNOWLEDGMENTS

We would like to thank the Brazilian agencies São Paulo Research Foundation (FAPESP)—Grant Nos. 2011/19296-1, 2014/07043-0, and 2015/50122-0—and CNPq—Grant Nos. 458425/2014-1 and 141192/2016-0—for their financial support to this work.

[1]G. Y. Antar, G. Counsell, Y. Yu, B. Labombard, and P. Devynck, Phys. Plasmas **10**, 419 (2003).
[2]G. Y. Antar, S. I. Krasheninnikov, P. Devynck, R. P. Doerner, E. M. Hollmann, J. A. Boedo, S. C. Luckhardt, and R. W. Conn, Phys. Rev. Lett. **87**, 065001 (2001).
[3]D. A. D'Ippolito, J. R. Myra, and S. J. Zweben, Phys. Plasmas **18**, 060501 (2011).
[4]T. A. Carter, Phys. Plasmas **13**, 010701 (2006).
[5]D. L. Toufen, F. A. C. Pereira, Z. O. Guimarães-Filho, I. L. Caldas, and K. W. Gentle, Phys. Plasmas **21**, 122302 (2014).
[6]C. Theiler, I. Furno, A. Kuenlin, P. Marmillod, and A. Fasoli, Rev. Sci. Instrum. **82**, 013504 (2011).

[7]K. W. Gentle and H. He, Plasma Sci. Technol. **10**, 284 (2008).
[8]A. A. Ferreira, M. V. A. P. Heller, I. L. Caldas, E. A. Lerche, L. F. Ruchko, and L. A. Baccala, Plasmas Phys. Controlled Fusion **46**, 669 (2004).
[9]O. E. Garcia, Phys. Rev. Lett. **108**, 265001 (2012).
[10]B. Labit, I. Furno, A. Fasoli, A. Diallo, S. H. Müller, G. Plyushchev, M. Podestà, and F. M. Poli, Phys. Rev. Lett. **98**, 255002 (2007).
[11]D. L. Toufen, Z. O. Guimarães-Filho, I. L. Caldas, J. D. Szezech, S. Lopes, R. L. Viana, and K. W. Gentle, Phys. Plasmas **20**, 022310 (2013).
[12]C. P. Ritz, E. J. Powers, T. L. Rhodes, R. D. Bengtson, K. W. Gentle, H. Lin, P. E. Phillips, A. J. Wootton, D. L. Brower, N. C. Luhmann, Jr., W. A. Peebles, P. M. Schoch, and R. L. Hickok, Rev. Sci. Instrum. **59**, 1739 (1988).
[13]B. Li and R. D. Hazeltine, Phys. Rev. E **73**, 065402(R) (2006).
[14]H. Johnsen, H. L. Pcseli, and J. Trulsen, Phys. Fluids **30**, 2239 (1987).
[15]A. V. Filippas, R. D. Bengston, G. X. Li, M. Meier, C. P. Ritz, and E. J. Powers, Phys. Plasmas **2**, 839 (1995).
[16]F. A. C. Pereira, D. L. Toufen, Z. O. Guimarães-Filho, I. L. Caldas, and K. W. Gentle, Plasmas Phys. Controlled Fusion **58**, 054007 (2016).
[17]D. Desideri and G. Serianni, Rev. Sci. Instrum. **69**, 2354 (1998).
[18]I. Furno, B. Labit, A. Fasoli, F. M. Poli, P. Ricci, C. Theiler, S. Brunner, A. Diallo, J. P. Graves, M. Podestà, and S. H. Müller, Phys. Plasmas **15**, 055903 (2008).
[19]B. Nold, T. T. Ribeiro, M. Ramisch, Z. Huang, H. W. Müller, B. D. Scott, U. Stroth, and ASDEX Upgrade Team, New J. Phys. **14**, 063022 (2012).
[20]M. Podesta, A. Fasoli, B. Labit, M. McGrath, S. H. Müller, and F. M. Poli, Plasmas Phys. Controlled Fusion **47**, 1989 (2005).
[21]A. H. Nielsen, J. J. Rasmussen, J. Madsen, G. S. Xu, V. Naulin, J. M. B. Olsen, M. Løiten, S. K. Hansen, N. Yan, L. Tophøj, and B. N. Wan, Plasmas Phys. Controlled Fusion **59**, 025012 (2017).
[22]S. I. Krasheninnikov, Phys. Lett. A **380**, 3905 (2016).
[23]Y. Zhang and S. I. Krasheninnikov, Phys. Plasmas **23**, 124501 (2016).